

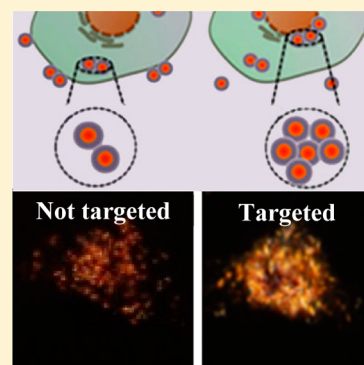
## Biological Targeting of Plasmonic Nanoparticles Improves Cellular Imaging via the Enhanced Scattering in the Aggregates Formed

Mena Aioub,<sup>†</sup> Bin Kang,<sup>†,‡</sup> Megan A. Mackey, and Mostafa A. El-Sayed\*

Laser Dynamics Laboratory, School of Chemistry and Biochemistry, Georgia Institute of Technology, Atlanta, Georgia 30332, United States

### Supporting Information

**ABSTRACT:** Gold nanoparticles (AuNPs) demonstrate great promise in biomedical applications due to their plasmonically enhanced imaging properties. When in close proximity, AuNPs plasmonic fields couple together, increasing their scattering cross-section due to the formation of hot spots, improving their imaging utility. In the present study, we modified the AuNPs surface with different peptides to target the nucleus and/or the cell as a whole, resulting in similar cellular uptake but different scattering intensities. Nuclear-targeted AuNPs showed the greatest scattering due to the formation of denser nanoparticle clusters (i.e., increased localization). We also obtained a dynamic profile of AuNP localization in living cells, indicating that nuclear localization is directly related to the number of nuclear-targeting peptides on the AuNP surface. Increased localization led to increased plasmonic field coupling, resulting in significantly higher scattering intensity. Thus, biochemical targeting of plasmonic nanoparticles to subcellular components is expected to lead to more resolved imaging of cellular processes.



### SECTION: Plasmonics, Optical Materials, and Hard Matter

In recent years, the use of nanoparticles in the biomedical field has increased greatly due to their small size and unique physical, optical, and chemical properties.<sup>1–4</sup> In particular, gold and silver metallic nanoparticles have been extensively studied due to their unique interaction with electromagnetic radiation, owing to their characteristic localized surface plasmon resonance (LSPR).<sup>5–8</sup> The LSPR arises from the coherent oscillation of conduction band electrons, in resonance with the incident light of a particular frequency, which depends on the dielectric function of the metal, that of the medium, as well as the size, shape, and composition of the nanoparticle.<sup>5,9</sup> The LSPR results in a remarkably strong enhancement of the electromagnetic field localized at the nanoparticle surface, which is utilized in surface-enhanced spectroscopy<sup>10</sup> and solar energy applications.<sup>11–13</sup> Additionally, the enhanced electric field (plasmonic field) of one nanoparticle can interact with that of an adjacent nanoparticle in close proximity, resulting in plasmon coupling.<sup>14–17</sup> The interparticle coupling leads to an intense enhancement of the plasmonic field relative to that of a single nanoparticle.<sup>17,18</sup> The LSPR of the coupled nanoparticles is red-shifted to longer wavelengths from the LSPR of a single nanoparticle, with a magnitude that depends on the proximity of the nanoparticles. Thus, the plasmon shift gives a measure of the distance between nanoparticles.<sup>14,15,19,20</sup>

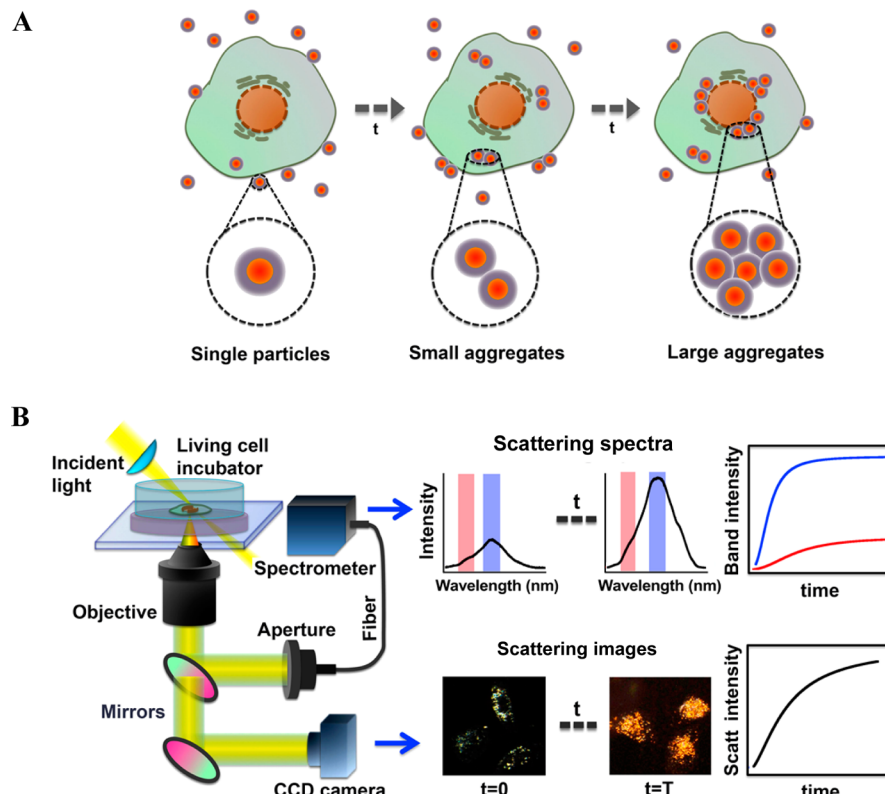
Gold nanoparticles (AuNPs) in particular have been increasingly utilized in a variety of biomedical fields, such as cellular imaging,<sup>21</sup> drug delivery,<sup>22</sup> and photothermal cancer therapy,<sup>23</sup> due not only to their plasmonic properties, but also to their relatively low toxicity and facile surface chemistry.<sup>2</sup> For many of these biomedical applications, gold nanoparticles often

need to be delivered intracellularly, and their nanoscale size allows AuNPs to be internalized by various types of cells through several endocytic processes.<sup>24–26</sup> This can be achieved by chemical modification of the AuNP surface with targeting ligands, such as the cancer cell membrane targeting peptide (RGD), to selectively deliver AuNPs into cancer cells through receptor-mediated endocytosis.<sup>24,27,28</sup> Also, chemical modification with a nuclear localization sequence (NLS) peptide can selectively deliver AuNPs to the cell nucleus.<sup>25,29–32</sup> Once AuNPs are internalized by cells, they are transported through subcellular vesicles and may accumulate in endosomes or lysosomes near the nucleus. During intracellular transport and localization, nanoparticles accumulate in subcellular components at different concentrations, which may depend on the size, shape, and most importantly, the surface chemistry of the nanoparticle. Therefore, understanding the localization of nanoparticles is critical to understanding their fundamental interactions within cells and improving their design for biomedical applications. To this end, the accumulation of AuNPs in endosomes and lysosomes has been observed by cryo-TEM,<sup>33,34</sup> but the direct observation of the dynamics of nanoparticle localization in living cells still remains a challenge. Our group has previously observed the cellular uptake of gold nanoparticles by live-cell plasmonically enhanced Rayleigh scattering imaging techniques, which take advantage of the subcellular localization of AuNPs, resulting in the enhancement

Received: May 30, 2014

Accepted: July 5, 2014

Published: July 5, 2014

Scheme 1. Schematic of Nanoparticle Localization by the PERSIS System<sup>a</sup>

<sup>a</sup>(A) Schematic representation of gold nanoparticle localization within cells during the process of cellular uptake; (B) Diagram of the experimental setup and the measurement of nanoparticle localization dynamics by PERSIS.

of AuNP Rayleigh scattering,<sup>35–38</sup> but the dynamics of this AuNP localization remains unknown.

In the present work, we have built a novel instrument and studied the cellular uptake and subcellular localization of AuNPs within living cells, in real-time, via single-cell plasmonically-enhanced Rayleigh-scattering imaging spectroscopy (PERSIS). This approach takes advantage of the characteristic optical properties of plasmonic AuNPs, namely, their ability to strongly scatter light, and the coupling of their plasmonic fields when particles come into close proximity. By monitoring the enhanced Rayleigh (elastic) scattering of different surface-modified AuNPs, the subcellular localization dynamics can be studied in real time. We have shown that the localization of AuNPs is dependent on the specific surface modification of the nanoparticles. Varying the amounts of the RGD and NLS peptides on the AuNP surface did not lead to a significant difference in the number of AuNPs internalized by the cancer cells, but large differences in the scattering intensity were observed due to the different surface modifications causing changes in AuNP localization within cells. Targeting AuNPs to the nucleus of cells increased the level of aggregation, leading to an increase in the total light scattered and a redshift to longer wavelengths, indicating enhanced coupling of the plasmonic fields due to decreased interparticle separation. Increasing the amount of NLS also caused the AuNPs to localize more rapidly, indicating that nuclear-targeted AuNPs may be more effective as imaging agents for biomedical applications, due to their greater light scattering ability and faster subcellular localization. This suggests that targeting subcellular components leads to greater localization, which offers an effective method of enhanced imaging using plasmonic nanoparticles.

**Synthesis of AuNPs with Different Biochemical Surface Properties.** For these studies, spherical AuNPs, approximately 30 nm in diameter, were synthesized by the citrate reduction method (Figure S1, Supporting Information).<sup>39</sup> The citrate-capped AuNPs were stabilized with polyethylene glycol thiol (mPEG-SH<sub>5k</sub>) to prevent nonspecific interactions under physiological conditions.<sup>28</sup> The PEG-AuNPs were then modified with RGD (arginine–glycine–aspartic acid) and NLS (nuclear localization signal) peptides. The RGD peptide allows for receptor-mediated endocytosis of AuNPs by targeting  $\alpha\beta\delta$  integrins, which are overexpressed on the surface of human oral squamous carcinoma (HSC-3) cells.<sup>28</sup> The NLS peptide has a characteristic KKKRK (lysine–lysine–arginine–lysine) sequence, which binds importins in the cytoplasm of the cell, allowing for translocation of AuNPs to the nucleus.<sup>25,29,30</sup> Peptide conjugation was utilized to design three different surface-modified AuNPs: RGD-AuNPs, RGD<sub>1</sub>/NLS<sub>1</sub>-AuNPs having equal amounts of RGD and NLS peptides, and RGD<sub>1</sub>/NLS<sub>10</sub>-AuNPs with RGD<sub>1</sub>/NLS<sub>10</sub>-AuNPs containing 10 times the NLS content of RGD<sub>1</sub>/NLS<sub>1</sub>-AuNPs. Previous work has shown that both RGD and NLS peptides indeed promote cellular uptake and localization of AuNPs at the nucleus,<sup>38,40,41</sup>

**PERSIS Design and Technique.** Since the endocytosis of AuNPs results in specific subcellular localization, we can observe the plasmonic coupling of single particles as they are internalized and come in proximity with other AuNPs.<sup>42,43</sup> As represented by Scheme 1A, the degree of AuNP localization within cells can vary. At the early stages of cellular uptake, the nanoparticles bind to receptors on the cell surface and are internalized into the cytoplasm to form small clusters of

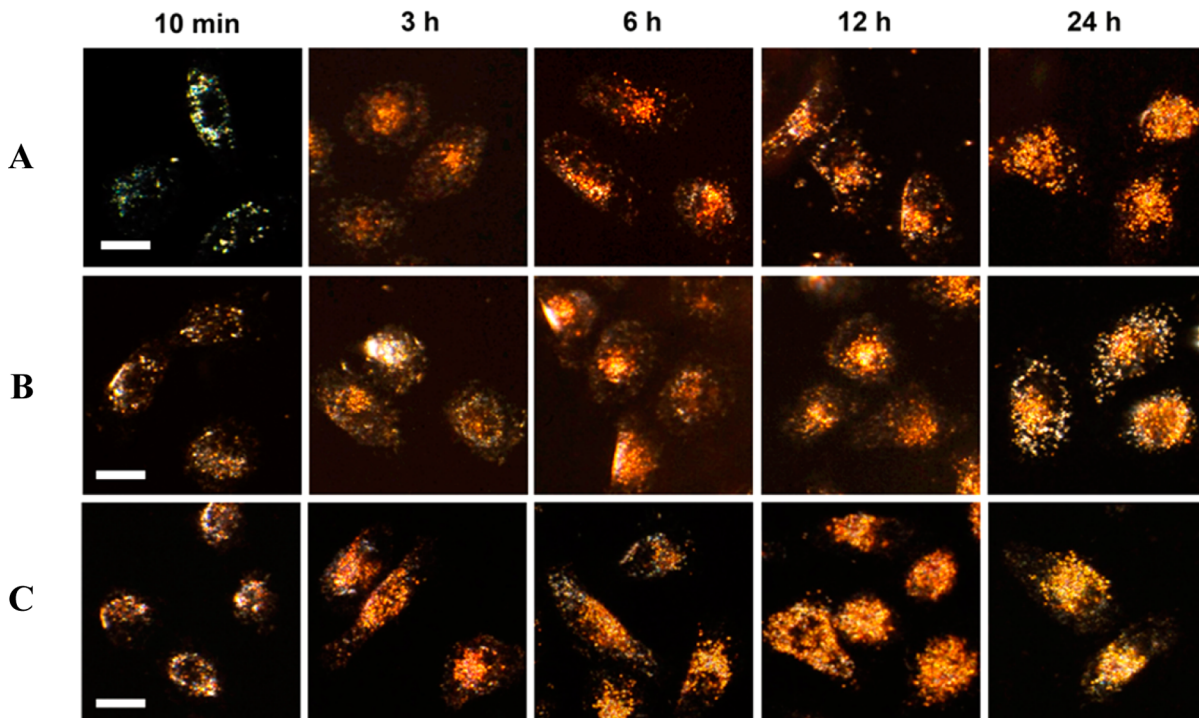


**Figure 1.** Real-time Rayleigh scattering dark-field images of cellular uptake of gold nanoparticles with different surface modifications: (A) RGD-AuNPs, (B) RGD<sub>1</sub>/NLS<sub>1</sub>-AuNPs, (C) RGD<sub>1</sub>/NLS<sub>10</sub>-AuNPs. Scale bar: 10  $\mu$ m.

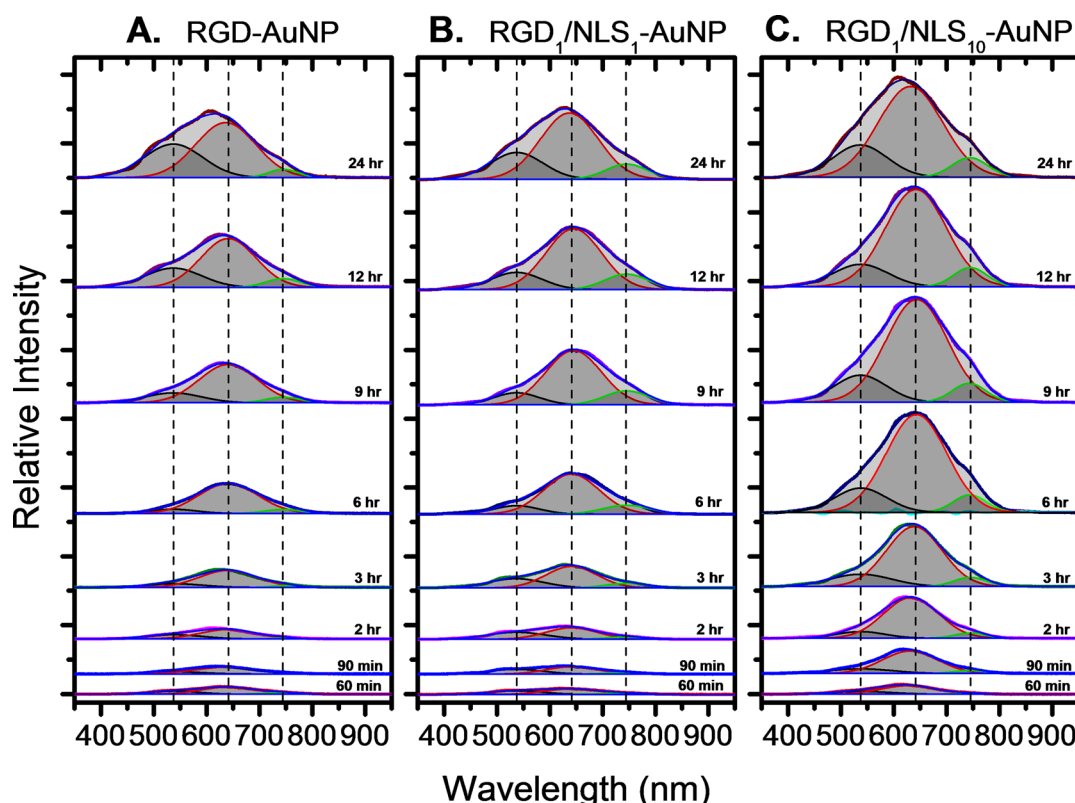


**Figure 2.** Real-time Rayleigh scattering spectra of AuNP uptake and localization within living cells for (A) RGD-AuNPs, (B) RGD<sub>1</sub>/NLS<sub>1</sub>-AuNPs, and (C) RGD<sub>1</sub>/NLS<sub>10</sub>-AuNPs. The deconvoluted peaks show the plasmonic scattering bands of single nanoparticles (538 nm), small AuNP clusters (641 nm), and large AuNP clusters (745 nm) and the center of the Gaussian fits are denoted by dashed lines.

particles.<sup>44</sup> This results in a redshift in the surface plasmon band from the single nanoparticle wavelength (538 nm) to longer wavelengths (641 nm), due to coupling of the plasmonic

fields between AuNPs as they localize and aggregate.<sup>44,45</sup> Subsequently, the AuNPs begin to form larger clusters as they accumulate in the endosomes or lysosomes and localize at the

perinuclear region,<sup>43,44</sup> causing a further shift in the plasmon band to even longer wavelengths (745 nm).<sup>46</sup> By monitoring the coupling of the plasmon bands, observed as a redshift in the LSPR, the dynamics of nanoparticle uptake and localization in single living cells can be followed in real time with our single-cell plasmon-enhanced Rayleigh scattering imaging spectroscopy (PERSIS) technique. Shown in Scheme 1B, our PERSIS system is composed of a homemade live cell incubator, a spectrometer to collect Rayleigh scattering spectra, and a dark-field microscope with an attached CCD camera to record the Rayleigh scattering images. This allows for the real-time monitoring of AuNP uptake and localization in living cells, by analyzing the scattering intensity in dark-field images and the plasmon band redshift of the Rayleigh scattering spectra over time.

**Localization Kinetics Using Plasmonically-Enhanced Rayleigh Scattering.** To ensure that changes in the observed scattering intensity were due to AuNP uptake (and not influenced by cell death), a treatment concentration of 0.4 nM AuNP in culture media was chosen for these studies. After 24 h, the viability of treated cells was measured using an XTT cell viability assay, and no significant cell death was observed from the three AuNP designs studied (Figure S3). Due to the  $\alpha\beta$  integrin targeting ability of RGD, all three AuNP samples studied also demonstrated similar levels of overall uptake ( $\sim 30\%$ , Figure S4). However, the intracellular localization of the different AuNPs varied based on the AuNP surface modification. As suggested by the live-cell Rayleigh-scattering dark field images in Figure 1, the AuNPs containing NLS peptide (Figure 1B,C) show higher AuNP localization at the nucleus compared to AuNPs without NLS (Figure 1A). Additionally, an increase in NLS peptide content (RGD<sub>1</sub>/NLS<sub>10</sub>-AuNPs) results in a more rapid localization rate of AuNPs at the nucleus (Figure 1C).

From these Rayleigh scattering dark-field images, our PERSIS technique allows us to obtain Rayleigh scattering spectra of AuNPs in living cells. Accordingly, spectra were collected for the various AuNPs tested over a 24 h period as shown in Figure 2. The entire spectrum obtained at each time point was integrated to give the total scattering intensity for each different surface modified AuNP, and is shown in Figure 3. From these integrated scattering intensities, we calculated a scattering half-time (see Supporting Information) for each different surface-modified AuNP to estimate the rate at which the AuNPs localize within cells. RGD-AuNPs were found to have a scattering half-time of 11.4 h, while RGD<sub>1</sub>/NLS<sub>1</sub>-AuNPs exhibited a faster scattering half-time of 6.7 h. RGD<sub>1</sub>/NLS<sub>10</sub>-AuNPs had the fastest scattering half-time of just 2.9 h. In addition to the faster half-time, indicating more rapid AuNP localization within cells, the RGD<sub>1</sub>/NLS<sub>10</sub>-AuNPs exhibit a significantly higher overall scattering intensity after 24 h, compared to that of RGD-AuNPs and RGD<sub>1</sub>/NLS<sub>1</sub>-AuNPs. This indicates that higher concentrations of NLS on the AuNP surface leads to an increased concentration of localized AuNPs at the perinuclear region, as evidenced by their more rapid increase in scattering, greater scattering intensity, and greater interparticle coupling of the plasmonic fields (i.e., greater intensity of the red-shifted plasmon peaks).

**AuNP Localization Dynamics.** The overall scattering spectrum shown in Figure 3 not only describes the total amount of light scattered by the different AuNPs in cells over time, but it can also provide a detailed dynamic profile of AuNP aggregation and localization. This subcellular localization results in the formation of AuNP clusters with smaller interparticle

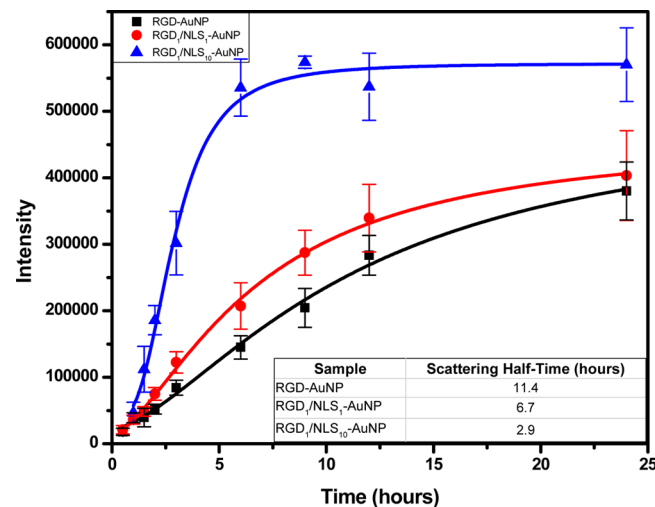


**Figure 3.** Dependence of the rate of increase of the scattered light intensity on the type of nanoparticle surface capping material, shown as the mean  $\pm$  s.e.m. of three independent experiments. This figure shows that the higher the concentration of NLS (the nuclear localization sequence), the higher the observed rate of the scattered light intensity increases. The calculated scattering half-times are given above for RGD-AuNPs (black,  $R^2 = 0.993$ ), RGD<sub>1</sub>/NLS<sub>1</sub>-AuNPs (red,  $R^2 = 0.997$ ), and RGD<sub>1</sub>/NLS<sub>10</sub>-AuNPs (blue,  $R^2 = 0.989$ ).

separations, leading to stronger coupling of their plasmonic fields and therefore, large red-shifted plasmon peaks. Thus, the total scattering spectrum obtained was fit to multiple Gaussians, allowing its deconvolution into three components: (1) AuNP monomers indicated by the plasmon band at 538 nm, (2) small AuNP clusters (with higher local concentrations of AuNPs, relative to AuNP monomers, which do not have interacting plasmonic fields), having a plasmon band at 641 nm, and (3) larger clusters of AuNPs (with the highest local AuNP concentration, indicating even greater coupling between the plasmonic fields of AuNPs in close proximity) give scattering at the longest wavelength of the 745 nm plasmon band (all are denoted with the dashed lines in Figure 2). Although the spectrum for each different AuNP contains these three components, the bands vary significantly based on the AuNP surface modification, indicating varying degrees of localization (i.e., different local concentrations of AuNPs within cells). In order to compare these bands for the different surface modified AuNPs and obtain detailed information on their degree of localization, the small (641 nm) and large (745 nm) AuNP cluster bands were integrated to give their total scattering intensities, as shown in Figure 4A,B, respectively. From these integrated scattering intensities, we again calculated a scattering half-time (see Supporting Information) for each different surface modified AuNP tested, to give a measure of how quickly the different AuNPs with different surface biochemical capping become localized.

During the formation of smaller AuNP clusters (Figure 4A), RGD-AuNPs and RGD<sub>1</sub>/NLS<sub>1</sub>-AuNPs showed similar scattering intensities after 24 h. However, RGD<sub>1</sub>/NLS<sub>1</sub>-AuNPs had a shorter small cluster half-time of 5.4 h, compared to 6.4 h for the AuNPs without the NLS peptide. The RGD<sub>1</sub>/NLS<sub>10</sub>-AuNPs were found to have the shortest small cluster half-time of 2.7 h, while showing a scattering intensity almost twice as large as that of the small cluster. This suggests that the increased amount of NLS peptides enhanced the rate of formation of small AuNP clusters at the perinuclear region.

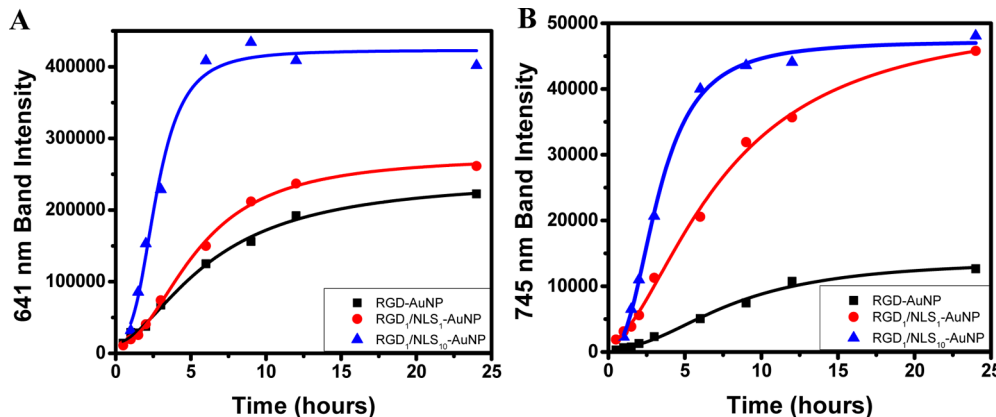


**Figure 4.** Dynamics of scattered light intensity for bands of (A) small AuNP clusters at 641 nm and (B) large AuNP clusters at 745 nm. Localization half-times of small AuNP clusters were calculated to be 6.4 h for RGD-AuNPs (black,  $R^2 = 0.995$ ), 5.4 h for RGD<sub>1</sub>/NLS<sub>1</sub>-AuNPs (red,  $R^2 = 0.997$ ), and 2.7 h for RGD<sub>1</sub>/NLS<sub>10</sub>-AuNPs (blue,  $R^2 = 0.979$ ). Localization half-times of large AuNP clusters were calculated to be 8.1 h for RGD-AuNPs (black,  $R^2 = 0.989$ ), 7.4 h for RGD<sub>1</sub>/NLS<sub>1</sub>-AuNPs (red,  $R^2 = 0.996$ ), and 3.3 h for RGD<sub>1</sub>/NLS<sub>10</sub>-AuNPs (blue,  $R^2 = 0.996$ ).

During the formation of the larger AuNP clusters (Figure 4B), NLS-modified particles (RGD<sub>1</sub>/NLS<sub>10</sub>-AuNPs and RGD<sub>1</sub>/NLS<sub>1</sub>-AuNPs) showed similar scattering intensities after 24 h. However, the AuNPs containing more NLS peptides (RGD<sub>1</sub>/NLS<sub>10</sub>-AuNPs) exhibited a shorter large cluster half-time of 3.3 h, compared to the 7.4 h for AuNPs containing less NLS peptide. Again, we attribute the shorter half-time to the increase in NLS peptides on the AuNP surface, enhancing the rate of nanoparticle localization at the nucleus or the nuclear membrane. The RGD-AuNPs were found to have the longest large cluster half-time of 8.1 h, while demonstrating a large aggregate scattering intensity almost five times smaller than the AuNPs bound to the NLS peptides. These results suggest that nuclear-targeted AuNPs tend to form more dense clusters having larger scattering cross sections, as they are bound to the small perinuclear region, than those not targeted to subcellular regions.

In conclusion, we have developed an instrument and demonstrated its use of PERSIS to monitor the uptake and localization dynamics of plasmonic AuNPs with different capping materials. The AuNPs surface modification greatly affected their localization and led to decreased interparticle separation between AuNPs, causing great enhancement of the scattered light and a red-shift in their observed plasmonic spectral peak to longer wavelengths. Nuclear-targeted AuNPs, directed to the smaller volume of the nucleus, were found to localize more rapidly than those not targeted to the nucleus of the cancer cells. This also leads to the formation of more dense clusters having more hot spots between the nanoparticles. Hot spots are known to have much more enhanced plasmonic fields leading to stronger scattering and thus better imaging of the region targeted by the nanoparticles. Increasing the concentration of the NLS peptides on the AuNP surface increased the localization rate and the concentration of the plasmonic nanoparticles at the NLS target in the cell. It is clear that this technique is not limited to studying the nuclear region. Various peptides are known to target different cellular components and the addition of a terminal thiol group would make it possible to conjugate the AuNPs for enhanced imaging at the selected location in the cell.

As a final point, the scattering enhancement due to AuNP localization is a result of overlap between the nanoparticles plasmonic fields. This does not necessarily require strong

chemical bonding between the capping materials on individual nanoparticles. To investigate this, cells were grown overnight, incubated with AuNPs for 24 h, washed, and finally, lysed to release the internalized AuNPs. The spectra of lysed AuNPs matched those of the initial AuNP monomers in water (data not shown), indicating that strong chemical aggregation of the nanoparticles did not occur upon targeting them to the nucleus. This is consistent with the fact that the thickness of the capping material is only  $\sim 8$  nm while the plasmonic field of the 30 nm AuNP decays over a  $\sim 30$  nm distance, allowing for their strong plasmonic field overlap away from the surface of each particle.

## ASSOCIATED CONTENT

### S Supporting Information

Gold nanoparticle TEM and UV-vis spectra, nanoparticle uptake, and detailed methods are included. This material is available free of charge via the Internet at <http://pubs.acs.org>.

## AUTHOR INFORMATION

### Corresponding Author

\*Mailing address: Department of Chemistry and Biochemistry, Georgia Institute of Technology, 901 Atlantic Drive, Atlanta, GA, 30332-0400. Adjunct Professor: Department of Chemistry, Faculty of Science, King Abdulaziz University, Jeddah, Saudi Arabia. E-mail: melsayed@gatech.edu.

### Present Address

<sup>‡</sup>(B.K.) College of Material Science and Technology, Nanjing University of Aeronautics and Astronautics, Nanjing, 210016, P.R. China.

### Author Contributions

<sup>†</sup>(M.A. and B.K.) Equal contribution.

### Notes

The authors declare no competing financial interest.

## ACKNOWLEDGMENTS

The authors wish to acknowledge the support of the National Institutes of Health - National Cancer Institute under Grant No. U01CA151802. M.A. also wishes to acknowledge the support of the U.S. Department of Education GAANN fellowship.

## ■ REFERENCES

- (1) Jain, P. K.; Huang, X. H.; El-Sayed, I. H.; El-Sayed, M. A. Noble Metals on the Nanoscale: Optical and Photothermal Properties and Some Applications in Imaging, Sensing, Biology, and Medicine. *Acc. Chem. Res.* **2008**, *41*, 1578–1586.
- (2) Dreaden, E. C.; Alkilany, A. M.; Huang, X. H.; Murphy, C. J.; El-Sayed, M. A. The Golden Age: Gold Nanoparticles for Biomedicine. *Chem. Soc. Rev.* **2012**, *41*, 2740–2779.
- (3) Burda, C.; Chen, X. B.; Narayanan, R.; El-Sayed, M. A. Chemistry and Properties of Nanocrystals of Different Shapes. *Chem. Rev.* **2005**, *105*, 1025–1102.
- (4) Kelly, K. L.; Coronado, E.; Zhao, L. L.; Schatz, G. C. The Optical Properties of Metal Nanoparticles: The Influence of Size, Shape, and Dielectric Environment. *J. Phys. Chem. B* **2003**, *107*, 668–677.
- (5) Link, S.; El-Sayed, M. A. Spectral Properties and Relaxation Dynamics of Surface Plasmon Electronic Oscillations in Gold and Silver Nanodots and Nanorods. *J. Phys. Chem. B* **1999**, *103*, 8410–8426.
- (6) Reinhard, B. M.; Sheikholeslami, S.; Mastroianni, A.; Alivisatos, A. P.; Liphardt, J. Use of Plasmon Coupling to Reveal the Dynamics of DNA Bending and Cleavage by Single EcoRV Restriction Enzymes. *Proc. Natl. Acad. Sci. U.S.A.* **2007**, *104*, 2667–2672.
- (7) Rong, G. X.; Wang, H. Y.; Skewis, L. R.; Reinhard, B. M. Resolving Sub-Diffraction Limit Encounters in Nanoparticle Tracking Using Live Cell Plasmon Coupling Microscopy. *Nano Lett.* **2008**, *8*, 3386–3393.
- (8) Aaron, J.; Travis, K.; Harrison, N.; Sokolov, K. Dynamic Imaging of Molecular Assemblies in Live Cells Based on Nanoparticle Plasmon Resonance Coupling. *Nano Lett.* **2009**, *9*, 3612–3618.
- (9) El-Sayed, M. A. Some Interesting Properties of Metals Confined in Time and Nanometer Space of Different Shapes. *Acc. Chem. Res.* **2001**, *34*, 257–264.
- (10) Schatz, G. C. Theoretical Studies of Surface Enhanced Raman Scattering. *Acc. Chem. Res.* **1984**, *17*, 370–376.
- (11) Kamat, P. V. Meeting the Clean Energy Demand: Nanostructure Architectures for Solar Energy Conversion. *J. Phys. Chem. C* **2007**, *111*, 2834–2860.
- (12) Standridge, S. D.; Schatz, G. C.; Hupp, J. T. Distance Dependence of Plasmon-Enhanced Photocurrent in Dye-Sensitized Solar Cells. *J. Am. Chem. Soc.* **2009**, *131*, 8407–8409.
- (13) Knight, M. W.; Wang, Y. M.; Urban, A. S.; Sobhani, A.; Zheng, B. Y.; Nordander, P.; Halas, N. J. Embedding Plasmonic Nanostructure Diodes Enhances Hot Electron Emission. *Nano Lett.* **2013**, *13*, 1687–1692.
- (14) Jain, P. K.; El-Sayed, M. A. Surface Plasmon Coupling and Its Universal Size Scaling in Metal Nanostructures of Complex Geometry: Elongated Particle Pairs and Nanosphere Trimers. *J. Phys. Chem. C* **2008**, *112*, 4954–4960.
- (15) Jain, P. K.; Huang, W. Y.; El-Sayed, M. A. On the Universal Scaling Behavior of the Distance Decay of Plasmon Coupling in Metal Nanoparticle Pairs: A Plasmon Ruler Equation. *Nano Lett.* **2007**, *7*, 2080–2088.
- (16) Lin, S.; Li, M.; Dujardin, E.; Girard, C.; Mann, S. One-Dimensional Plasmon Coupling by Facile Self-Assembly of Gold Nanoparticles into Branched Chain Networks. *Adv. Mater.* **2005**, *17*, 2553–2559.
- (17) Gunnarsson, L.; Rindzevicius, T.; Prikulis, J.; Kasemo, B.; Kall, M.; Zou, S. L.; Schatz, G. C. Confined Plasmons in Nanofabricated Single Silver Particle Pairs: Experimental Observations of Strong Interparticle Interactions. *J. Phys. Chem. B* **2005**, *109*, 1079–1087.
- (18) Slaughter, L. S.; Wu, Y. P.; Willingham, B. A.; Nordlander, P.; Link, S. Effects of Symmetry Breaking and Conductive Contact on the Plasmon Coupling in Gold Nanorod Dimers. *ACS Nano* **2010**, *4*, 4657–4666.
- (19) Sonnichsen, C.; Reinhard, B. M.; Liphardt, J.; Alivisatos, A. P. A Molecular Ruler Based on Plasmon Coupling of Single Gold and Silver Nanoparticles. *Nat. Biotechnol.* **2005**, *23*, 741–745.
- (20) Reinhard, B. M.; Siu, M.; Agarwal, H.; Alivisatos, A. P.; Liphardt, J. Calibration of Dynamic Molecular Ruler Based on Plasmon Coupling between Gold Nanoparticles. *Nano Lett.* **2005**, *5*, 2246–2252.
- (21) Loo, C.; Lowery, A.; Halas, N.; West, J.; Drezek, R. Immunotargeted Nanoshells for Integrated Cancer Imaging and Therapy. *Nano Lett.* **2005**, *5*, 709–711.
- (22) Kang, B.; Afifi, M. M.; Austin, L. A.; El-Sayed, M. A. Exploiting the Nanoparticle Plasmon Effect: Observing Drug Delivery Dynamics in Single Cells via Raman/Fluorescence Imaging Spectroscopy. *ACS Nano* **2013**, *7*, 7420–7427.
- (23) Hirsch, L. R.; Stafford, R. J.; Bankson, J. A.; Sershen, S. R.; Rivera, B.; Price, R. E.; Hazle, J. D.; Halas, N. J.; West, J. L. Nanoshell-Mediated Near-Infrared Thermal Therapy of Tumors under Magnetic Resonance Guidance. *Proc. Natl. Acad. Sci. U.S.A.* **2003**, *100*, 13549–13554.
- (24) Castel, S.; Pagan, R.; Mitjans, F.; Piulats, J.; Goodman, S.; Jonczyk, A.; Huber, F.; Vilardo, S.; Reina, M. RGD Peptides and Monoclonal Antibodies, Antagonists of  $\alpha_v$ -Integrin, Enter the Cells by Independent Endocytic Pathways. *Lab. Invest.* **2001**, *81*, 1615–1626.
- (25) Tkachenko, A. G.; Xie, H.; Liu, Y. L.; Coleman, D.; Ryan, J.; Glomm, W. R.; Shipton, M. K.; Franzen, S.; Feldheim, D. L. Cellular Trajectories of Peptide-Modified Gold Particle Complexes: Comparison of Nuclear Localization Signals and Peptide Transduction Domains. *Bioconjugate Chem.* **2004**, *15*, 482–490.
- (26) Gao, H.; Shi, W.; Freund, L. B. Mechanics of Receptor-Mediated Endocytosis. *Proc. Natl. Acad. Sci. U.S.A.* **2005**, *102*, 9469–9474.
- (27) Zitzmann, S.; Ehmann, V.; Schwab, M. Arginine-Glycine-Aspartic Acid (RGD)-Peptide Binds to Both Tumor and Tumor-Endothelial Cells in Vivo. *Cancer Res.* **2002**, *62*, 5139–5143.
- (28) Xue, H.; Atakilit, A.; Zhu, W. M.; Li, X. W.; Ramos, D. M.; Pytela, R. Role of the  $\alpha v \beta 6$  Integrin in Human Oral Squamous Cell Carcinoma Growth in Vivo and in Vitro. *Biochem. Biophys. Res. Commun.* **2001**, *288*, 610–618.
- (29) Tkachenko, A. G.; Xie, H.; Coleman, D.; Glomm, W.; Ryan, J.; Anderson, M. F.; Franzen, S.; Feldheim, D. L. Multifunctional Gold Nanoparticle-Peptide Complexes for Nuclear Targeting. *J. Am. Chem. Soc.* **2003**, *125*, 4700–4701.
- (30) Escriou, V.; Carriere, M.; Scherman, D.; Wils, P. NLS Bioconjugates for Targeting Therapeutic Genes to the Nucleus. *Adv. Drug Delivery Rev.* **2003**, *55*, 295–306.
- (31) Feldherr, C. M.; Akin, D. Regulation of Nuclear Transport in Proliferating and Quiescent Cells. *Exp. Cell. Res.* **1993**, *205*, 179–186.
- (32) Nakielny, S.; Dreyfuss, G. Transport of Proteins and RNAs in and out of the Nucleus. *Cell* **1999**, *99*, 677–690.
- (33) Jiang, W.; Kim, B. Y. S.; Rutka, J. T.; Chan, W. C. W. Nanoparticle-Mediated Cellular Response Is Size-Dependent. *Nat. Nanotechnol.* **2008**, *3*, 145–150.
- (34) Chithrani, B. D.; Ghazani, A. A.; Chan, W. C. W. Determining the Size and Shape Dependence of Gold Nanoparticle Uptake into Mammalian Cells. *Nano Lett.* **2006**, *6*, 662–668.
- (35) Austin, L. A.; Kang, B.; El-Sayed, M. A. A New Nanotechnology Technique for Determining Drug Efficacy Using Targeted Plasmonically Enhanced Single Cell Imaging Spectroscopy. *J. Am. Chem. Soc.* **2013**, *135*, 4688–4691.
- (36) El-Sayed, I. H.; Huang, X.; El-Sayed, M. A. Surface Plasmon Resonance Scattering and Absorption of Anti-EGFR Antibody Conjugated Gold Nanoparticles in Cancer Diagnostics: Applications in Oral Cancer. *Nano Lett.* **2005**, *5*, 829–834.
- (37) Huang, X.; El-Sayed, I. H.; El-Sayed, M. A. Applications of Gold Nanorods for Cancer Imaging and Photothermal Therapy. *Methods Mol. Biol.* **2010**, *624*, 343–357.
- (38) Kang, B.; Mackey, M. A.; El-Sayed, M. A. Nuclear Targeting of Gold Nanoparticles in Cancer Cells Induces DNA Damage, Causing Cytokinesis Arrest and Apoptosis. *J. Am. Chem. Soc.* **2010**, *132*, 1517–1519.
- (39) Frens, G. Controlled Nucleation for Regulation of Particle-Size in Monodisperse Gold Suspensions. *Nat. Phys. Sci.* **1973**, *241*, 20–22.
- (40) Austin, L. A.; Kang, B.; Yen, C. W.; El-Sayed, M. A. Plasmonic Imaging of Human Oral Cancer Cell Communities During

Programmed Cell Death by Nuclear-Targeting Silver Nanoparticles. *J. Am. Chem. Soc.* **2011**, *133*, 17594–17597.

(41) Mackey, M. A.; Saira, F.; Mahmoud, M. A.; El-Sayed, M. A. Inducing Cancer Cell Death by Targeting Its Nucleus: Solid Gold Nanospheres Versus Hollow Gold Nanocages. *Bioconjugate Chem.* **2013**, *24*, 897–906.

(42) Kang, B.; Austin, L. A.; El-Sayed, M. A. Real-Time Molecular Imaging Throughout the Entire Cell Cycle by Targeted Plasmonic-Enhanced Rayleigh/Raman Spectroscopy. *Nano Lett.* **2012**, *12*, 5369–5375.

(43) Chithrani, B. D.; Chan, W. C. W. Elucidating the Mechanism of Cellular Uptake and Removal of Protein-Coated Gold Nanoparticles of Different Sizes and Shapes. *Nano Lett.* **2007**, *7*, 1542–1550.

(44) Nativo, P.; Prior, I. A.; Brust, M. Uptake and Intracellular Fate of Surface-Modified Gold Nanoparticles. *ACS Nano* **2008**, *2*, 1639–1644.

(45) Storhoff, J. J.; Lazarides, A. A.; Mucic, R. C.; Mirkin, C. A.; Letsinger, R. L.; Schatz, G. C. What Controls the Optical Properties of DNA-Linked Gold Nanoparticle Assemblies? *J. Am. Chem. Soc.* **2000**, *122*, 4640–4650.

(46) Su, K. H.; Wei, Q. H.; Zhang, X.; Mock, J. J.; Smith, D. R.; Schultz, S. Intercparticle Coupling Effects on Plasmon Resonances of Nanogold Particles. *Nano Lett.* **2003**, *3*, 1087–1090.